Thermo-mechanical behavior of titanium beryllide pebble beds at ambient temperature

Joerg Reimann[a,*], Benjamin Fretz[b], Ramil Gaisin[a], Aniceto Goraieb[b], Jae-Hwan Kim[c], Suguru Nakano[c], Masaru Nakamichi[c], Pavel Vladimirov[a]

[a] Karlsruhe Institute of Technology, Institute for Applied Materials, Hermann-von-Helmholtz-Platz 1, 76344 Eggenstein-Leopoldshafen, Germany

[b] Karlsruhe Beryllium Handling Facility (KBHF GmbH), Hermann-von-Helmholtz-Platz 1, 76344 Eggenstein-Leopoldshafen, Germany

[c] National Institutes for Quantum and Radiological Science and Technology, 2-166 Omotedate, Obuchi, Rokkasho, Aomori 039-3212, Japan

ABSTRACT

The thermomechanical behavior of titanium beryllide pebble beds was investigated experimentally at ambient temperature in helium. The pebbles consist of a mixture of $TiBe_{12}$ and Ti_2Be_{17} titanate beryllide phases and a small residual amount of Be phase, denominated as Be-7.7Ti.

For purposes of comparison, experiments in air and helium atmosphere were also conducted with Be, Al_2O_3 and orthosilicate pebble beds. The pebble beds were compressed uniaxially up to 4.5MPa; the effective thermal conductivity was measured using the hot wire technique. The stress-strain curves do not differ significantly for the different granular materials in contrast to the effective thermal conductivity k. Whereas for Be pebble beds k increases strongly with increasing stress (about 600% for the uniaxial stress of 4MPa), the increase is much smaller for the other granular materials (about 60% for Be-7.7Ti at 4MPa). The main reason for the large differences is the much lower thermal conductivity of the solid materials. Another influence exists because the other materials are mechanically harder resulting in smaller contact surfaces.

As long as the thermal conductivity of other beryllide materials is significantly lower than that of Be, comparable results are expected as for Be-7.7Ti.

It is argued that similar results are expected for single phase $TiBe_{12}$ pebble beds. Because of the harder behavior compared to Be-7.7Ti pebbles, the effective thermal conductivity might be slightly smaller. Although the above reasonings suggest that a phase mixture can be used instead of the single phase $TiBe_{12}$, this issue has to be investigated in more detail.

*Corresponding author
Email address: reimann-langhans@web.de (Joerg Reimann)

1. INTRODUCTION

In most helium cooled ceramic breeder blankets for fusion power reactors, the beryllium containing neutron multiplier and the breeder material are envisaged in the form of pebbles. In the ITER fusion reactor aimed to show a proof of concept, pure beryllium is the prime candidate material. For advanced fusion reactors, beryllium intermetallic compounds, beryllides, such as $TiBe_{12}$, VBe_{12}, $ZrBe_{13}$ are promising candidates. These materials, developed first for airborne and space applications [1], became of interest for fusion reactor applications because of the higher upper temperature limits, lower chemical reactivity, lower swelling under neutron irradiation, and better tritium release [2-7]. In parallel to the first beryllide characterizations using disks, the production of beryllide pebbles was developed by the rotating electrode process, REP, using electrodes fabricated by the plasma sintering process [8]. First, the aim was to produce single phase $TiBe_{12}$ as electrode material. Although this was achieved quite well using the stoichiometric composition of Be-7.7at%Ti, it proved that the remelting and solidification during the REP caused a structural change with the result that the pebbles consisted of about 11% of Be; 34% of $TiBe_{12}$ and 55% of Ti_2Be_{17} [9]. In order to obtain single phase $TiBe_{12}$, a homogenization treatment at 1473K for more than 8h was added, however, resulting in a non-negligible void production [9]. Because beryllide electrodes proved to be very brittle and, therefore, are not suited for an industrial process, electrodes with a higher ductility were anticipated. With electrodes consisting of about 50% of Be and beryllide [10], the same pebble composition was obtained as in [9]. Finally, it was no longer attempted to generate beryllides during the plasma sintering process but to generate electrodes consisting of a Be-Ti composite with a sufficient mechanical strength for REP [11].

An economically interesting alternative is the electrode production by hot extrusion [12]. Titanium beryllide pebble beds originating from the latter process are the topic of this paper.

During blanket operation, temperature differences and different thermal expansion coefficients between pebble beds and structural materials result in constrained strains, which cause elastic and plastic pebble deformations. The modelling of this thermal-mechanical interaction between pebble beds and structural materials is mandatory for every blanket design, requiring as an input important pebble bed quantities as a function of temperature such as i) the deformation behavior (stress-strain, σ-ε, relation and ii) the effective thermal conductivity, k.

There is a large database for both the granular ceramic breeder materials (the reader is referred to the corresponding literature) and beryllium pebble beds, see e.g. [13,14]. Because sufficient amounts of beryllide pebbles became available only recently, no thermo-mechanical data existed, except thermal conductivity data for non-compressed vanadium beryllide pebble beds [15].

The thermo-mechanical pebble bed behavior is generally investigated by combining uniaxial compression tests (UCTs) with a method to measure the effective thermal conductivity, *k*. In respect to the latter, either steady-state methods [13,14,16] or the transient hot wire method (HWM) were applied [17,18,19]. The HWM is a relatively simple technique, especially suited for materials with rather small thermal conductivities, k in the order of 1 W/(mK). However, it was proven [18,19] that it can be also applied for compressed beryllium pebble beds with *k* in the order of 10 W/(mK).

Because titanium beryllide pebble beds, produced by the hot extrusion process followed by REP, are the main topic of the present investigations, the production sequence is briefly described, for details, see [12]. In the Karlsruhe Beryllium Handling Facility, KBHF, beryllium and titanium powders with stoichiometric compositions corresponding to $TiBe_{12}$ (Be-7.7at.%Ti) were filled first in niobium capsules, outgassed and sealed and then inserted into CuCrZr capsules. Extrusion was performed at the Extrusion Research and Development Center, Technical University of Berlin in air atmosphere at 650 °C using an 8 MN extrusion press with a ram speed of about 10 mm/s. In order to produce ductile REP electrodes, the extrusion process was carried out again in such a way that the extruded rods consisted of a Be-7.7at.%Ti composite. Back in the KBHF, the Be-Ti rods were dismantled, cut into pieces with lengths appropriate for REP electrodes, and sent to the National Institutes for Quantum and Radiological Science and Technology, QST, for the pebble production. Rotating speeds of 5000~7000 rpm and electric currents of 60~70 A were applied depending on the diameter of the Be-Ti rods. The resulting beryllide pebbles were sent back to KIT for further experiments.

For the present pebbles, again, a composition similar to that in [10] was obtained, see Section 3.1. A homogenization treatment was not performed, therefore, in the following this titanium beryllide is designated as Be-7.7Ti.

2. EXPERIMENTAL SET-UP

The pebbles surfaces were investigated using optical microscopy on a KEYENCE VHX 2000 and Reichert-Jung MeF3. The cross sections were studied using scanning electron microscopy on a Zeiss Merlin. Energy-dispersive X-ray spectroscopy (EDS) was used to analyze the contents of Ti and other impurities on the cross sections of the pebbles.

The small amount of pebble bed material necessitated the use of the set-up already required previously for the same reason [19]. For accuracy assessments of the obtained results, experiments with other granular materials such as Be, orthosilicate, Osi, and Al_2O_3 pebbles were carried out as well in order compare these results with other references. All experiments were performed at ambient temperature, $T_a \approx 20$ °C; experiments at elevated temperatures are being

prepared. Additional to the investigations with granular materials, the thermal conductivity of water was measured, using a water gel (5g Agar/1l water) in order to avoid free convection [20].

Table 1: Characteristic properties of investigated granular materials (T=20°C)

Mat	d mm	ρ g/cm^3	k_s, Ref W/(mK)
Be-7.7Ti	1	2.279	40*, [7]
Be	1	1.855	185, [23]
Al_2O_3	1.1	2.700	26.7, [20]
Osi	0.34	2.383	2.9, [24]
helium: k =0.154W/(mK) , air: k=0.027 W/(mK)			

*Value for $TiBe_{12}$

Table 1 contains characteristic data of the investigated granular materials. The mean pebble diameters were about 1 mm, except for Osi with d = 0.34 mm. The Be pebbles, fabricated by NGK, originated from recent work [13,14], as well as the Al_2O_3 pebbles which were already used in [21]. The EU candidate Osi pebble material was recently investigated in detail [22,23]. The table contains also the thermal conductivity k_s of the solid materials at ambient temperature. These data are required for comparisons, see Sections 3.4ff. For the Be-7.7Ti pebbles, the density was measured by pycnometry; for k_s the value for single phase $TiBe_{12}$ from [7] was assumed. In the near future, this value will be checked by k_s results from other investigations with composites of $TiBe_{12}$ and Be. The Al_2O_3 material was selected because k_s is quite close to that of $TiBe_{12}$.

Figure 1 shows the cylindrical stainless steel container (inner diameter D: 60 mm, height H: 50 mm, wall thicknesses: 10 mm) with the HW probe located horizontally 23 mm above the cylinder bottom. The figure shows also the arrangement of the container inside the press together with the stainless steel lid containing the four displacement transmitters, separated by 90°, for measuring individually pebble bed strains ε. This system, already used in previous work [13,14,18,19], has the advantage that i) strains are directly measured; without involving other components of the press, and ii) it provides a sensitive control if after vibration the lid plate is in a horizontal position in the press. Already height differences of a few tenths of a mm at the circumference of the lid result in remarkably differing strain signals indicating a non-homogeneous bed compression with the consequence that the σ–ε curves evaluated with the mean strain values differ to those obtained with a horizontal lid plate. The uniaxial stress σ was measured using the force transmitter of the press.

The HW probe was manufactured in the central workshop of KIT, based on a more than twenty years old experience. It consists of two so-called “cold end” parts and, in between, the primary heating (HW) section. The three parts consist of coaxial wires within small tubes of 1 mm outer diameter and a wall thickness of 0.1 mm; separated by a MgO layer. The wires of the cold ends consist of Ni with a diameter of ≈ 0.4 mm; whereas the HW material is NiCr8020 with a diameter of

≈ 0.22 mm. The largest challenge during manufacturing is the connection of the two wires with different diameters. Because of industrial property rights, no further details are given. Finally, the tubes are connected by laser welding and two 0.25 mm diameter NiCr-Ni thermocouples, TCs, are laser-welded on the steel cladding surface; one in the middle; the other 8mm apart. This system is shifted through holes in the container wall, fixed at one side in order to allow for thermal expansion through the hole on the other side and finally connected with plugs.

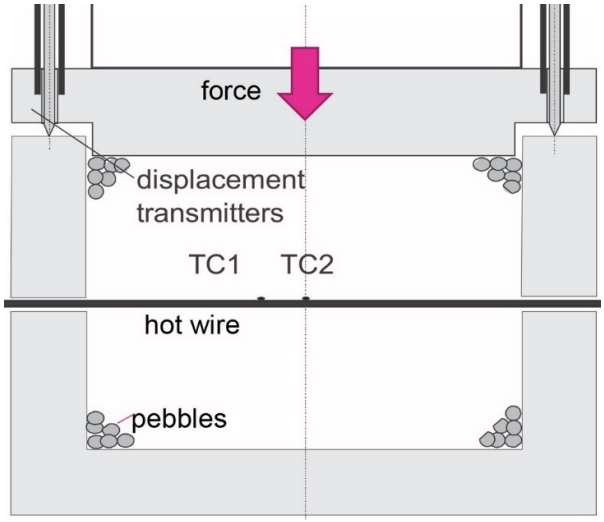

Fig. 1. HW container and strain measurement system.

The concept of the HW design is straightforward: the heat production in the cold ends should be small compared to that in the central heater. For the present HW probe with a HW length *L* of 53 mm, the electrical resistance in the cold ends was 7% of the HW resistance which agreed well with calculated values using manufacturer specifications.

The electric current *I* (A) of the constant current power supply is measured by means of a shunt outside of the glovebox whereas the voltage drop for the evaluation of the HW system resistance is measured at the HW plugs. For the calculation of the effective thermal conductivity, see Section 3, the HW resistance *R* is used, obtained by subtracting the cold end resistance from the measured total value.

As mentioned above, two TCs are laser-welded on the steel cladding surface at different positions. Originally, only the middle TC was foreseen for *k* measurements; the other one was anticipated for the detection of the starting influence of the finite container. It showed, however, that *k* evaluated from both TCs did not differ systematically in the relevant measurement time range; therefore, both TCs were used for *k* evaluation.

Because of the significant burden during pebble bed compression, the used HW systems have varying lifetimes. The failure of one, then two TCs can occur or the connection of the cold end and

HW wires starts to fail, indicated by a characteristic change of the electrical resistance. In the present investigations, one TC failed shortly before the completion of the experimental program.

Before starting experiments in the glovebox, experiments outside the glovebox in air atmosphere without compression were carried out with Osi and Al_2O_3 pebble beds and with the HW immersed in water gel. All pebble beds were vibrated before the HW measurements both inside and outside the glovebox using vibrators from Binder Magnete, Type 21 %0A-08A1.

The glovebox experiments were performed in helium atmosphere at 0.1 MPa. Only at the end of the experimental campaign, the glovebox was operated with air for compression experiments with Be and Al_2O_3 pebble beds. Due to the fact that the experiments were carried out at ambient temperature, there was no concern that the Be pebbles would become severely oxidized.

3. RESULTS

3.1 Pebble microstructure and pebbles images

Figure 2 represents the microstructure of the cross section of a Be-7.7Ti pebble consisting of coarse beryllide dendrites with 5–30 μm in diameter and up to 200–300 μm in length. The EDX

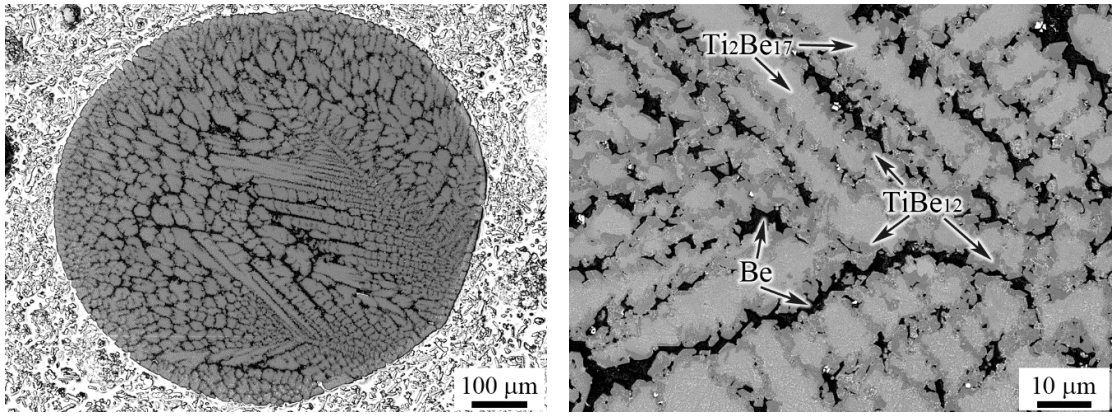

a) b)

Fig. 2. Microstructure of the cross-section of the Be-7.7Ti pebble: a) dendritic structure of the pebble, b) constituent phases in the increased view.

shows that the interdendritic space is formed by the beryllium phase, often containing pores and particles of beryllium oxide. The dendrites have Ti_2Be_{17} cores with $TiBe_{12}$ on the surface. The volume fractions of Be, $TiBe_{12}$, and Ti_2Be_{17} are approximately 11%, 40% and, 49%, respectively.

The obtained microstructure of pebbles is similar to that obtained earlier in [9,10, 26]. The increased content of beryllium can be explained by the peritectic reaction during solidification. In this case, the composition of the dendrite branch turns out to be supersaturated with titanium, and the interdendritic

space contains more beryllium. Homogenization heat treatment at 1200°C can transform beryllium and the Ti_2Be_{17} phase into $TiBe_{12}$ [9, 26], however, this heat treatment results in a higher porosity, predominantly in former places of the Be phase, which can facilitate brittle fracture of pebbles. On the other hand, residual beryllium in an amount up to 15% does not lead to the retention of a significant amount of tritium and does not cause severe swelling and pore formation under neutron irradiation [27]. The more ductile beryllium phase might also increase the overall ductility of pebbles, which is preferable in respect to the generation of larger contact surfaces, resulting in greater effective thermal conductivity values.

Pebble shapes, surface roughness, size distributions can affect both the packing fraction (ratio of pebble volume to pebble bed volume), γ, and the effective thermal conductivity k.

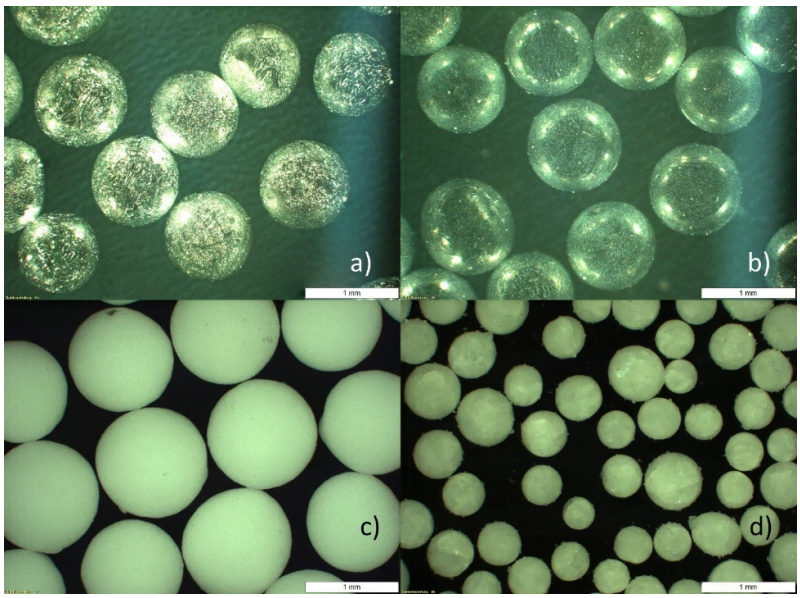

Fig. 3. Pebble samples, a) Be-7.7Ti, b) Be-NGK, c) Al_2O_3, d) Osi.

Figure 3 shows pictures of samples of the investigated granular materials, taken by a Reichert-Jung MeF3 optical microscope. All pebbles are of fairly spherical shape; some tiny satellite spheres are observed, resulting from the solidification process. The Osi pebbles have diameters between 0.25 and 0.65 mm with the mean diameter given in Table 1. The other pebbles have a smaller dispersity with tolerances of about 0.1 mm from the mean diameter.

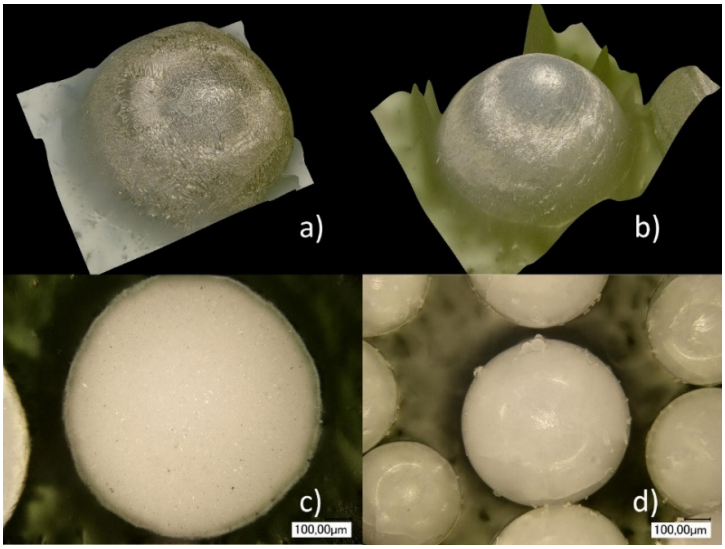

Fig. 4. Individual pebbles, a) Be-7.7Ti, b) Be-NGK, c) Al_2O_3, d) Osi.

Figure 4 presents pictures from individual pebbles, obtained with a KEYENCE VHX 2000 optical microscope. On the first look, Figs. 4a) and 4b) might be confusing by indicating crater-like surfaces. However, this impression is an optical illusion, caused solely by the microscope illumination (metallic surfaces are shiny; ceramic surfaces are dull). The surface of the Be-7.7Ti pebbles is rougher because of the dendritic structure compared to that of the Be pebbles. The presently used Be pebbles were already used in earlier compression tests [13,14] and the question was, if residual plastic deformations can be detected. This is not the case, and it can be concluded that earlier compression tests caused primarily elastic deformations and, if any, plastic deformations below the detection limit. The surfaces of the Al_2O_3 pebbles are smoother, even more than those of Osi pebbles.

3.2 HW operational regimes

The standard equation to calculate the effective thermal conductivity for the HWM is:

$$k=2.3Q/(2\pi L)(T_2-T_1)/(\log t_2-\log t_1) \quad (1),$$

where Q (W) is the electric power, given by RI^2, where I (A) is the HW electric current, and R (Ω) is HW electric resistance, compare Section 2. T is the temperature at a distinct point (here: the position of one of the thermocouples) and t is the elapsed time since switching on Q. Replacing the time t by $t^* = \log t$, Eq (1) becomes

$$k = 2.3Q/(2\pi L)(T_2-T_1)/(t^*_2-t^*_1) \quad (1a).$$

Plotting T as a function of t^*; k has to be evaluated in that region, where the temperature gradient becomes constant.

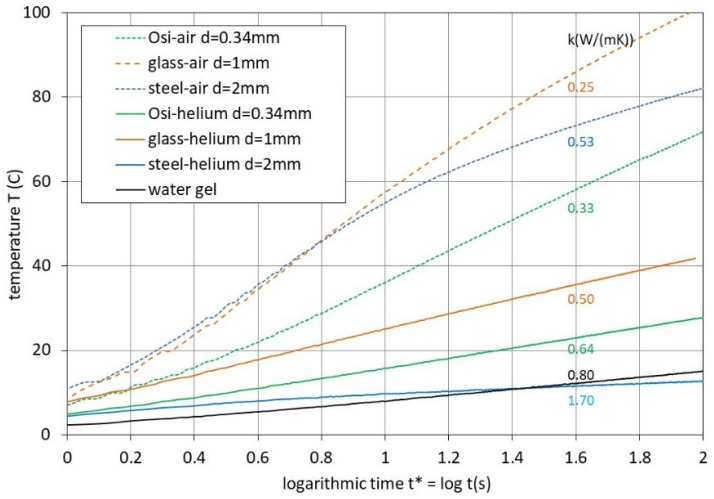

Fig. 5. HW temperature for different granular materials in air and helium and the HW immersed in water gel.

Figure 5 shows characteristic temperature distributions from previous nonpublished experiments and new measurements with water gel in order to demonstrate the influence of the pebble diameter *d*, respectively the heat transfer coefficient, *HTC*, between the granular material and the HW wall. For the HW immersed in water gel (pure conduction condition) no heat resistance exists at the wall interface (corresponding to an infinitely large *HTC* value). Because of this, the linear slope is reached very fast. When the HW is surrounded by a nonhomogeneous material such as the pebble bed, the pebbles contacting the HW have a different heat transfer characteristic (and packing structure) compared to the pebble bed zone farer away whose effective thermal conductivity is to be measured. For the modelling of temperature fields in finite containers, this is taken into account by using finite *HTC* values, see e.g. [18, 19, 22]. The lower the *HTC* value, the longer it takes until the constant slope $\Delta T/\Delta t^*$ is reached, see Fig. 5. This is most expressed for 2 mm steel spheres in air atmosphere and to a lesser extent for 1 mm glass spheres in air. For the small Osi pebbles, the slope becomes constant also for air atmosphere after a short time period For helium atmosphere with a much larger thermal conductivity k_g than that for air, the initial time period becomes small for all materials investigated; for details, see [18, 19, 22].

An important question is, if TCs fixed at the outside of the HW cladding have an impact on measured *k* values compared to the temperature measurement directly by the HW. In fact, TCs at the outside of the cladding can be in direct or non-direct contacts with pebbles which influences the initial time period. However, when temperature diffusion through the un-disturbed pebble bed zone becomes dominant, these initial effects play no longer any role.

In contrast to some results shown in Fig. 5, HW powers in the present experiments were chosen such that ΔT was in the order of 1°C for the relevant Δt^*.

In recent investigations [19] with beryllium pebble beds in helium atmosphere using pebble dimensions larger than 2 mm, effective thermal conductivities larger than 10 W/(mK) were measured. A detailed 2d and 3d simulation of the experimental set-up was performed and a correlation was developed, where the determination of k was a function of t^* in such a way that t^* decreased with increasing k.

In the present work, the main interest concerns pebble beds with ≈ 1 mm diameter pebbles and considerably lower k values. In the present paper, therefore, the HW operational regimes are assessed following the procedure recently used [22], based on older work [28-30]: Eq (1) is a truncation of the full solution, the truncation error becomes negligible (less than 1%) for

$$t_{tr} > 5d_{HW}^2/\alpha \qquad (2),$$

where d_{HW} is the diameter of the HW probe, α is the thermal diffusivity of the granular material, $\alpha = k_s/(\rho c_p)$, k_s is the solid material thermal conductivity, ρ is the apparent density, $\rho = \gamma\rho_s$ and c_p are the specific heat of the solid material.

The influence of the HW length on the axial heat flow becomes negligible for

$$t_L < 0.0633L^2/(4\alpha) \qquad (3),$$

and the influence of the finite radial boundary becomes negligible for

$$t_H < 0.25(H/2)^2/\alpha \qquad (4).$$

Eqs. (3) and (4) are valid for a cylindrical container with the HW at the axis. For the present setup, there is no rotational symmetry; as characteristic dimension in Eq (4), H/2 is taken.

The axial heat flow error in the HW is negligible for $L/d_{HW} > 25$ which is well fulfilled (L/d_{HW} = 53).

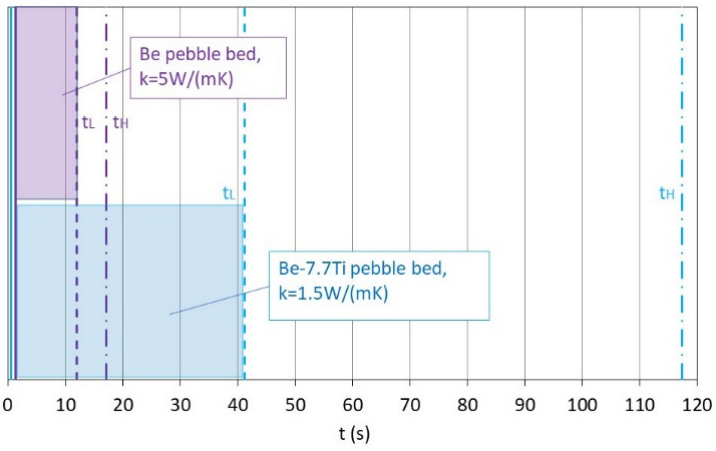

Fig. 6. Operational HW regimes

Figure 6 shows the different operational regimes for a Be-7.7Ti pebble bed with an assumed effective thermal conductivity of 2 W/(mK) and for a Be pebble bed with k = 5 W/(mK). In both cases, the truncation error becomes neglible for t > 3s. For the Be-7.7Ti pebble bed, the upper operational time is limited to 41s by Eq (3). For Be with k = 5 W/(mK), however, this limit is reduced to 12s.

In the following, Eq (1a) is not directly used but the procedure from [19] is applied where the temperature distribution is fitted for the appropriate time span by an expression of the type

$$T = Ct^{*a} \quad (5),$$

where C and a are constants. This fitting is advantageous for smoothening small T fluctuations and, furthermore, enables the direct determination of k by using the gradient dT/dt^* resulting in

$$k = 2.3Q/(2\pi L)t^{*(1-a)}/(aC) \quad (6).$$

For Be pebble beds, k was evaluated for t^* = 1; for all other granular materials, the value t^* = 1.477 was used, corresponding to t = 30s. It should be noted, that the results differ marginally for the different t* values.

3.3 Packing fractions

The HW method presumes a uniform packing structure in an infinitely large packing volume. In practice, such a structure exists only in a fraction of the finite volume. Close to walls, the particles start to arrange in a structured order which influences both the local packing fraction and the HW signal. The local packing fraction differs the most in the wall layer adjacent to walls. Here, in the wall zone with d/2 thickness the packing fraction cannot exceed the maximum value of $\gamma_{d/2}$ = 0.6 for hexagonal dense sphere packing, compare e.g. [31,32]. In practice, this value is smaller, in previous experiments with Al_2O_3 pebbles [32] with a comparable diameter spread as in the present 1 mm pebble experiments, the value $\gamma_{d/2}$ = 0.5 was determined. The packing fraction in the inner, non-disturbed volume γ_i is then approximately determined by

$$\gamma_i = (\gamma V - \gamma_i V_{d/2})/V_i \quad (7),$$

where γ is the packing fraction determined with the total packing volume V, $V_{d/2}$ is the volume of all wall layers with d/2 thickness and $V_i = V - V_{d/2}$. For the present setup and 1 mm pebbles γ_i is increased by only ≈ 0.007 compared to γ, for the smaller Osi pebbles this difference is even smaller. The differences can become remarkably greater for larger particles and slender containers.

Although the effect of the HW volume on the packing fraction is negligible it is worth to mention that the HW with a diameter ratio of pebble to HW diameter of ≈ 1 represents also a distinct disturbance

of the packing structure as demonstrated in [31]. Again, the effect of this disturbance on the HW temperature signal disappears after the short initial measurement period, compare Section 3.2.

The packing fractions of the vibrated pebble beds were between 0.615 and 0.635. No distinct differences between the different granular materials were observed despite of the different pebble morphologies shown in Figs. 3 and 4. More detailed experiments with a larger set-up are desirable.

3.4 Effective thermal conductivity for water and non-compressed pebble beds

Table 2 contains results for the measured effective thermal conductivity for non-compressed pebble beds, k_0, as well as corresponding values found in literature, k_{ref}. For Be-7.7Ti and Al_2O_3 pebble beds, no other measurements were found, therefore, the Schlünder-Bauer-Zehner model, SBZ model [33] was applied which was already chosen as basis in previous work [11,12]. However, a slightly modified version was used, SBZmod, by evaluating the SBZ parameter B with the correlation from [34], according to the recommendation by [35]. Furthermore, the value of the SBZ parameter ρ_k^2 was selected to 0.00005 for non-compressed pebble beds, as proposed previously by several authors, see e.g. [17,21]. For applying the SBZmod model for Be-7.7Ti pebble beds, the value for single-phase $TiBe_{12}$ was assumed [7]. The SBZ model values given in Table 2 were evaluated for γ = 0.625 and T = 20°C.

Table 2: Non-compressed pebble beds: Effective thermal conductivity from other references or SBZmod model, $k_{ref,}$ and ratio of mean value of measured k_0 to k_{ref} .

		helium, 0.1MPa		air, 0.1MPa	
Mat	d mm	k_{ref}, Ref W/(mK)	k_0/k_{ref}	k_{ref}, Ref W/(mK)	k_0/k_{ref}
Be-7.7Ti	1.0	1.64*, SBZmod	0.97		
Be	1.0	1.97, SBZmod,	1.05	0.74, SBZmod	1.18
Al_2O_3	1.1	1.55, SBZmod	0.96	0.49, SBZmod	0.71
Osi	0.34	0.89, [21]	1.10	0.38, [21]	0.90
water: k_{ref} = 0.607 W/(mK), [19]; k_0/k_{ref} = 1.27					

*with k_s for $TiBe_{12}$

Figure 7 shows k/k_{ref} for water and non-compressed pebble beds as a function of the HW electric current I. A clear dependency on I is not observed. The largest deviations exist for water with the mean value of k/0.608=1.29. The reason for these large deviations is unclear; perhaps caused by free convection flow effects, which might more easily occur using horizontal HWs; in [22] a mean value of 1.09 was measured with a vertical HW probe. For Be-7.7Ti the mean k value agrees fairly well with that of the SBZ model. Therefore, one can assume that k_s for Be-7.7Ti does not differ significantly from that for $TiBe_{12}$. For Be and Al_2O_3 pebble beds in helium the agreement is also satisfactory. In [15], $k \approx$ 2W/(mK) was obtained for Be pebble beds which agrees even better with the present results. For Al_2O_3 pebble beds in helium; one value, k = 1.7 W/(mK), was given in [21] which is even larger than the present measurements. For Osi pebble beds, the measurements agree reasonably with the correlations [22,23] both for helium and air atmospheres.

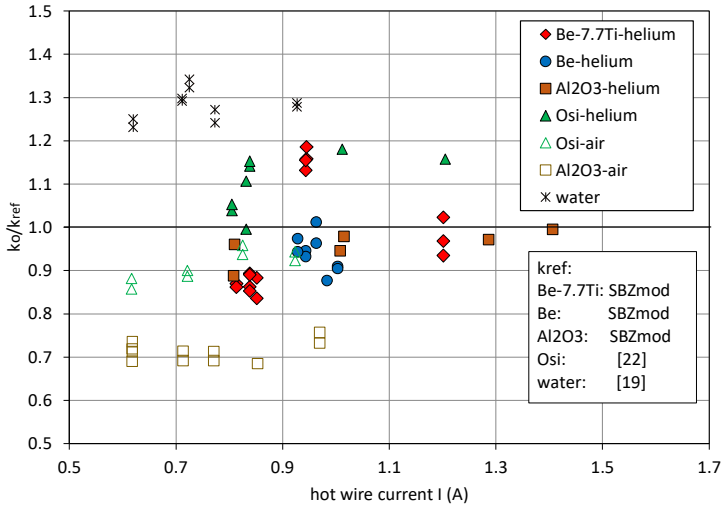

Fig. 7. k_0/k_{ref} for water and non-compressed pebble beds as a function of the HW electric current *I*.

Summarizing the results, it can be stated that for non-compressed pebble beds where comparisons are possible with data from other work, the agreement between measurements and results from other references is satisfactory, considering the restrictions of the used set-up, compare Section 2. All data points in Fig.8 are mean values of the two TCs. The estimated value of the measurement error for the used measurement system is estimated to 15%.

3.5 Stress-strain dependence of compressed pebble beds

Both experiments without compression and with compression were performed within the glovebox. In the latter case, the pebble beds were compressed by the piston of a press up to pressures of about 4.5 MPa. Maximum ramp rates were of 0.3 MPa/min. In UCTs, the piston pressure corresponds to the uniaxial stress σ; therefore, the latter term is used in the following. The σ values were increased stepwise and *k* was measured after each step. The number of *k* measurements was larger for the first stress increase period which is of special importance for blanket operation, compare [13,14]. After reaching the maximum σ value, σ was decreased stepwise to low values and two more cycles were carried out, again always in combination with HW measurements. In total, more than 20 compression tests were performed; experimental results with remarkably differing individual strain signals were discarded.

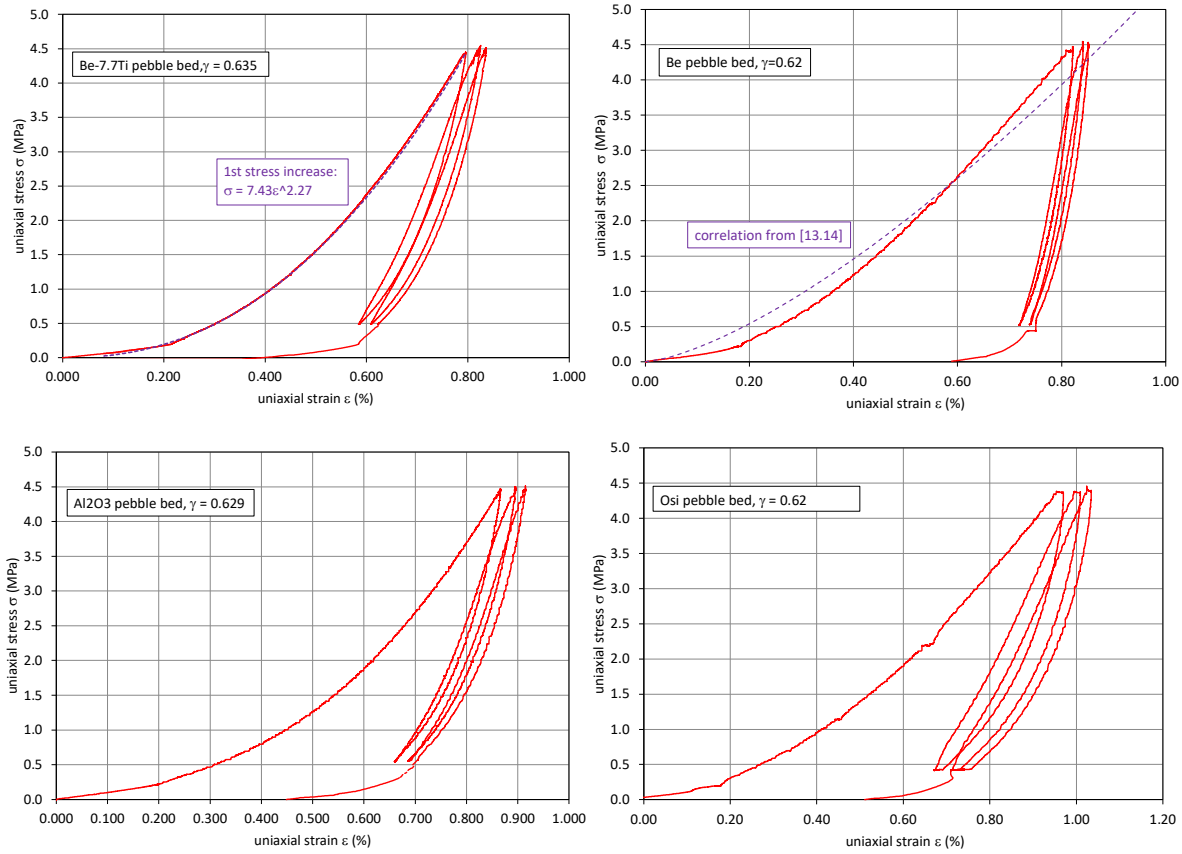

Fig. 8. Stress-strain curves for Be-7.7Ti, Be, Al_2O_3 and Osi pebble beds.

Figure 8 shows characteristic σ–ε curves for the different granular materials. Relatively small differences are observed and clear trends could not be attributed to the specific materials because the packing fraction varied as well. The curves are quite close to those measured previously using a larger set-up [13,14]. The first stress increase curve for Be-7.7Ti is fitted by:

$$\sigma(MPa) = 7.43\varepsilon(\%)^{2.27} \qquad (8).$$

3.5. **Effective thermal conductivity for compressed pebble beds: first stress increase period**

During the first stress increase period, pebbles rearrange and are subjected to elastic/plastic deformations. In earlier work with Be pebble beds [13,14], as prime parameter the strain ε was considered and the important result was that k increased linearly with ε. This behavior is also evident in Fig. 9 with k/k_0 as ordinate, where k_0 is the value for the non-compressed pebble bed. The data scatter is partly caused by the fact that results are exhibited from several experiments with slightly differing packing fractions. The most significant result is, that for Be pebble beds the increase of k/k_0 during compression is much greater than for Be-7.7Ti pebble beds.

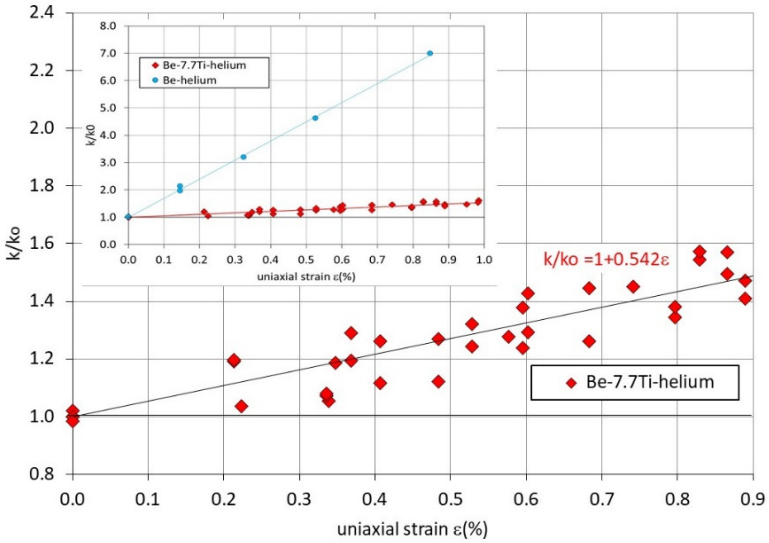

Fig. 9. Conductivity ratio k/k_0 as a function of strain for Be and Be-7.7Ti pebble beds.

In the following figures, as abscissa the uniaxial stress σ is used which eliminates the influence of different σ–ε relations for the different granular materials. Figure 10 represents results for all materials. Again, only Be pebble beds show a drastic increase of k with stress σ.

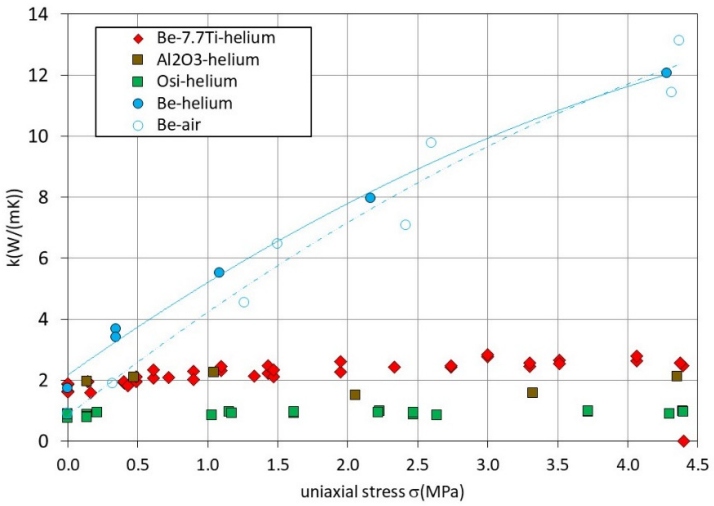

Fig. 10. Effective thermal conductivity as a function of stress.

Figure 11 depicts in more detail the results for moderate k values. For Osi pebble beds, the increase of k is negligible as measured first by [36] and confirmed recently by [22]. Be-7.7Ti pebble beds show a moderate increase, with $k/k_0 \approx 1.5$ at $\sigma = 4$MPa; the data are fitted by:

$$k/k_0 = 1+0.275\sigma^{0.441} \qquad (9).$$

Compared to Be-7.7Ti, for Al_2O_3 pebble beds, the increase is even smaller.

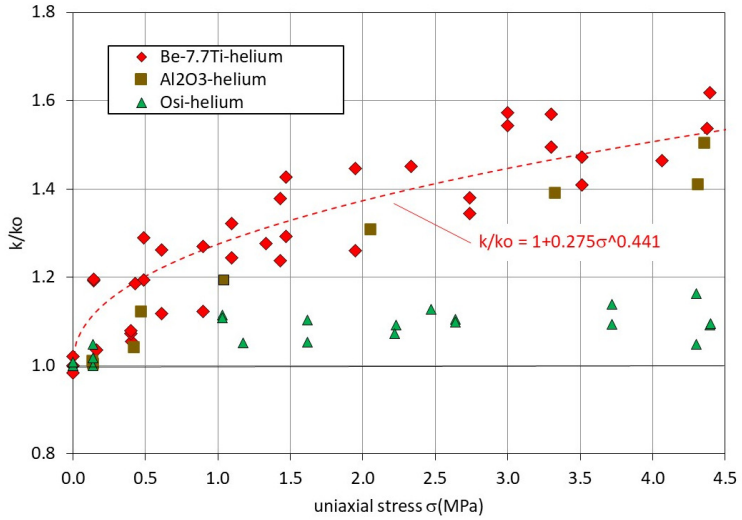

Fig. 11. Conductivity ratio k/k_0 as a function of stress.

In order to describe the differences between the different materials, the SBZ model [33] is used in combination with the correlations for Be pebble beds from previous work [13,14]. Here, the primary correlation was given as $k=f(T,\varepsilon)$. In the SBZ model, the compression is taken into account by the parameter ρ_k^2 which is the ratio of contact surfaces between pebbles to the pebble cross section. This parameter was fitted [13,14] as a function of strain by

$$\rho_k^2 = 0.0041\ \varepsilon(\%) + 0.0021\ \varepsilon(\%)^2 \quad . \qquad (7).$$

With the σ–ε relation for the first stress increase curve [13]:

$$\sigma(MPa) = 5.41\varepsilon(\%)^{1,43}, \qquad (8),$$

ρ_k^2 is expressed as a function of σ:

$$\rho_k^2 = 0.00126\sigma^{0.7} + 0.0002\sigma^{1.39} \qquad (9).$$

In Fig. 12, k/k_0 is evaluated for different values of k_s corresponding to those given in Table 1, for helium atmosphere at ambient temperature. It is demonstrated that the increase of k/k_0 with

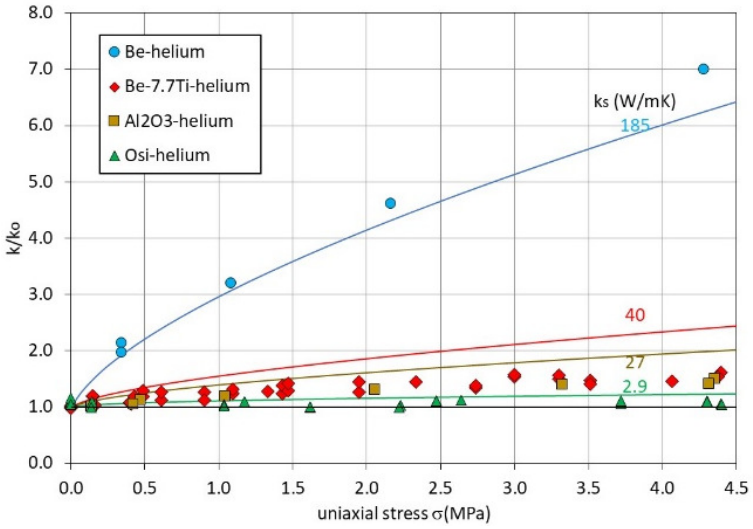

Fig. 12. Conductivity ratio k/k_0 for different k_s values.

increasing deformation reduces strongly with decreasing k_s. The agreement with measurements is also good for the present Be pebble bed experiments. For the other materials, the curves are generally higher than the measurements, especially for the Be-7.7Ti pebble beds. It should be repeated again, that the calculated curves are based on previous correlations for the more ductile Be pebbles. The differences between calculated curves and measurements for the Be-7.7Ti and Al_2O_3 pebble beds can be caused by the harder behavior of these materials, resulting in smaller contact surfaces compared to Be pebbles. For single phase TiBe12 pebble beds the results might be slightly lower because these pebbles are expected to be even more brittle than the Be-7.7Ti ones.

The results from Fig. 12 are also of significance for the use of other beryllides: As long as k_s is significantly smaller than that of Be, the increase of k with increasing stress is strongly reduced. For VBe_{12}, k_s = 29 W/(mK) was used in [8]; a value of 38 W/(mK) was measured in [7]; therefore $k=f(\sigma)$ is expected to be similar to that of Be-7.7Ti pebble beds.

Figure 10 shows also results for compressed Be pebble beds in air atmosphere. Compared to Be pebble beds in helium, the differences for small σ values are large because of the large difference between the thermal conductivities of two gases. With increasing compression, the measured differences reduce because again the heat transfer through the pebble contact surfaces becomes dominating.

3.6. **Effective thermal conductivity for compressed pebble beds: cycling behavior**

During the first stress decrease period and the following cycles mainly elastic deformation changes occur. However, zones of blocked pebble arrangements might still exist during the stress decrease periods with the consequence that the k/k_0 values as a function of σ are generally larger than the values for the first stress increase period. This effect was already observed for Be pebble beds [13,14] and exists also in the Be-7.7Ti experiments, as shown in Fig. 13. At σ_{max}, the k value obtained at the end of the first stress increase period is again reached at the end of subsequent cycles. This will change if at elevated temperatures thermal creep effects occur, compare [13,14].

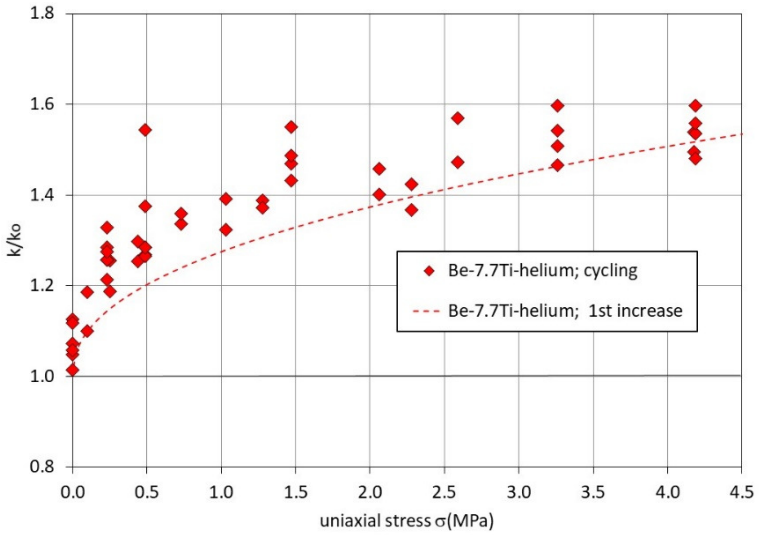

Fig. 13. Effective thermal conductivity for compressed Be-7.7Ti pebble beds during cycling.

4. Conclusions

The thermomechanical behavior of Be-7.7Ti pebble beds was investigated at ambient temperature in helium. The pebbles consist of a mixture of Be, and $TiBe_{12}$ and Ti_2Be_{17} titanates with volume fractions of 11%, 40%, and 49%, respectively.

For purposes of comparison, experiments in air and helium atmosphere were conducted also with Be, Al_2O_3 and Osi pebble beds. The stress-strain curves from UCTs do not differ significantly for the different granular materials in contrast to the effective thermal conductivity k. The k increase for Be-7.7Ti pebble beds with increasing stress is significantly smaller compared to Be pebble beds. For the uniaxial stress of 4 MPa, the increase is ≈ 60% compared to 600% for Be pebble beds. The main reason for this large difference is the much lower thermal conductivity of solid material Be-7.7Ti compared to Be. The greater mechanical hardness of the Be-7.7Ti pebbles can be also a contributing factor, which results in smaller contact surfaces.

It is argued that for single phase $TiBe_{12}$ pebble beds no remarkably different results are expected. Because of the expected harder behavior compared to Be-7.7Ti pebbles, the effective thermal conductivity might be slightly smaller.

For other beryllides with thermal conductivities k_s significantly smaller than that of Be, also small increases of k with increasing stress are expected. For VBe_{12}, k_s is close to the value of $TiBe_{12}$; therefore, $k = f(\sigma)$ is expected to be similar to that for Be-7.7Ti pebble beds.

It was argued that the use of Be-7.7Ti instead of single phase $TiBe_{12}$ should not result in a remarkably deteriorated behavior in respect to tritium retention and neutron irradiation induced swelling, instead, pebble ductility and density might be superior. These issues should be discussed in more detail including also other mechanisms where single phase beryllides show a superior behavior compared to Be in order to decide if a subsequent heat treatment of the Be-7.7Ti pebbles is advisable.

Corresponding investigations with Be-7.7Ti pebble beds at elevated temperatures are in preparation.

Acknowledgements

This work has been carried out within the framework of the EUROfusion Consortium and has received funding from the EURATOM research and training programme 2014-2018 and 2019-2020 under the grant agreement No 633053. The German Ministry for Education and Research (Bundesministerium für Bildung und Forschung – BMBF) funded the framework project of this paper under the grant number 03FUS0012, as a contribution to the “Broader Approach” activities. The responsibility for the contents of this publication is with the authors.

References

[1] K.A Walsh, Beryllium chemistry and processing, ASM International Materials Park, OH 44073-0002 (2009).

[2] L. A. Jacobson, R. A. Hanrahan, J. L. Smith, Chapter 3 Beryllides, Intermetallic Compounds; Vol. 3, Eds. J.H. Westbrook, R.L. Fleischer (2002) John Wiley & Sons, Ltd.

[3] H. Kawamura, T. Takahashi, N. Yoshida, V. Shestakov, Y. Ito, M. Uchida, H. Yamada, M. Nakamichi, E. Ishitsuka, Application of beryllium intermetallic compounds to neutron multiplier of fusion blanket, Fusion Eng. Des. 61-62 (2002) 391-397.

[4] M. Uchida, E. Ishitsuka, H. Kawamura, Thermal conductivity of neutron irradiated Be12Ti, Fusion Eng. Des. 69 (2003) 499-503.

[5] K. Munaka, H. Kawamura, M. Uchida, Surface reaction of titanium beryllide with water vapor, Fusion Eng. Des. 81 (2006) 993-998.

[6] M. Uchida, E. Ishitsuka, H. Kawamura, Tritium release properties of neutron-irradiated Be12Ti, J. Nucl. Mater. 307-311 (2002) 635-656.

[7] J. Reimann, C. Dorn, A. Goraieb, H. Harsch, W. Haws,P. Kurinskiy, R. Lindau, C. Linsmeier C. Linsmeier A. Moeslang, M. Rohde, Beryllides for Fusion, Symposium on Engineering, SOFE 2009, San Diego, USA, June 1-5 2009, IEEE CFP09SOF-PRT, 305-309.

[8] M. Nakamichi, J.H. Kim, Fabrication of beryllide pebble as advanced neutron multiplier, Fusion Eng. Des. 89 (7–8) (2014) 1304–1308.

[9] M. Nakamichi, J.H. Kim, Homogenization treatment to stabilize the compositional structure of beryllide pebbles, J. Nucl. Mater. 440 (1–3) (2013) 530–533.

[10] J.H. Kim, M. Nakamichi, Effect of titanium content on mechanical properties and reactivity of titanium beryllide pebbles, Fusion Eng. Des. 98–99 (2015) 1812-1816.

[11] M. Nakamichi, J.-H. Kim, Development of beryllide pebbles with low-hydrogen generation as advanced neutron multipliers, Fusion Eng. Des. 125 (2017) 537-540.

[12] P. Kurinskiy, H. Leiste, A. Goraieb, R. Rolli, S. Mueller, J. Reimann, A. Moeslang, “Production of Be-Ti and Be-Zr rods by extrusion and their characterization”; Fusion Eng. Des. 136 (2018) 49-52.

[13] J. Reimann, G. Piazza, Z. Xu, A. Goraieb, H. Harsch, Measurements of the thermal conductivity of compressed beryllium pebble beds, FZKA-7096 (Mai 2005).

[14] J. Reimann, G. Piazza, H. Harsch, Thermal conductivity of compressed beryllium pebble beds, Fusion Eng. Des., 81 (2006) 449-54

[15] M. Nakamichi, J-H. Kim, P. Kurinskiy, Characterization of vanadium beryllide pebble bed for the Japan DEMO blanket application, Fusion Eng. Des. 136 (2018) 125-127.

[16] A. Abou-Sena, A. Ying, M. Abdou, Experimental investigation and analysis of the effective thermal properites of beryllium packed beds, Fusion Science and Technology, Vol. 44, (2003) 79-84.

[17] M. Enoeda, K. Furuya, H. Takatsu, S. Kikuchi, T. Hatano, Effective thermal conductivity measurements of the binary pebble beds by hot wire method for the breeding blanket, Fusion Technology, Vol. 34, No. 3, Pt. 2, (1998) 877-881.

[18] J. Reimann, S. Hermsmeyer, G. Piazza, G. Wörner, Thermal conductivity measurements of deformed beryllium pebble beds by hot wire method, in: M. Yamawaki (Ed.), CBBI-9, Toki, Japan, September 27–29, 2000, Univ. of Tokyo, Tokyo, 2002, pp. 199–214.

[19] J. Reimann, B. Fretz, S. Pupeschi, Thermo-mechanical screening tests to qualify beryllium pebble beds with non-spherical pebbles, Fusion Eng. Des. Fusion Eng. Des. 98–99 (2015) 1851-1854

[20] ASTM Standard, Standard Test Method for Determination of Thermal Conductivity of Soil and Soft Rock by Thermal Needle Probe Procedure, Designation: D 5334 – 08.

[21] M. Dalle Donne, G. Sordon, Heat transfer in pebble beds, Fusion Technology Vol.17 (1990) 597-635.

[22] S. Pupeschi, Thermomechanical characterization of advanced ceramic breeder beds for fusion blankets, Thesis, KIT (2018).

[23] S. Pupeschi, R. Knitter, M. Kamlah, Effective thermal conductivity of advanced ceramic breeder pebble beds, Fusion Eng. Des.116 (2017) 73-80.

[24] M. Dalle Donne (compiler), European DEMO BOT solid breeder blanket, Kernforschungszentrum Karlsruhe Report KFK 5429, Nov 1994.

[25] B. Schultz, in: KfG contributions to the development of Demo relevant test blankets for NET/ITER,, ed. M. Dalle Donne, KFK 4927 (1991) 139

[26] V. Chakin, R. Rolli, R. Gaisin, P. Kurinskiy, J.-H. Kim, M. Nakamichi, Effect of heat treatment of titanium beryllide on tritium/hydrogen release, Fusion Eng. Des. 137 (2018) 165–171.

[27] V. Chakin, R. Rolli, R. Gaisin, U. Hoeppener-Kramar, M. Nakamichi, M. Zmitko, Tritium release and retention in beryllium and titanium beryllide after neutron irradiation up to damage doses of 23-38 dpa, Fusion Eng. Des. 161 (2020) 111-138.

[28] J. H. Blackwell, “A Transient-Flow Method for Determination of Thermal Constants of Insulating Materials in Bulk Part I—Theory”, J. of Appl. Phys. 25, 137 (1954); doi: 10.1063/1.1721592.

[29] J. H Blackwell, The axial flow error in the thermal conductivity probe, Can. J. Phys. 34, (1956), 412.

[30] P. Andersson, G. Backström, Thermal conductivity of solids under pressure by the transient hot wire method, Review of Scientific Instruments 47, 205 (1976); doi: 10.1063/1.1134581

[31] J. Reimann, J. Vicente, E. Brun, C. Ferrero, Y. Gan, A. Rack, X-ray tomography investigations of mono-sized sphere packing structures in cylindrical containers, Powder Technology 318 (2017) 471–483

[32] J. Reimann, J. Vicente, C. Ferrero, A. Rack, Y.Gan, 3d tomography analysis of the packing structure of spherical particles in slender prismatic containers, Int. J. Material Research 111(2020) 1, 65-77

[33] E. V. Schlünder, Particle heat transfer, Proc 7th Int. Heat Transfer Conf., München, Germany, September 6-10, 1982, Hemisphere Publ. Co. Vol. 1, RK10, (1982) 195-212,

[34] C.T. Hsu, P. Cheng, K.W. Wong, Modified Zehner–Schlünder models for stagnant thermal conductivity of porous media. Int. J. Heat and Mass Transfer 37 (1994) 2751–2759.

[35] W. van Antwerpen, C.G. du Toit, P.G. Rousseau, A review of correlations to model the packing structure and effective thermal conductivity in packed beds of monosized spherical particles, Nucl. Eng. Des. 240 (2010) 1803–1818.

[36] J. Reimann, S. Hermsmeyer, Thermal conductivity of compressed ceramic breeder pebble beds, Fusion Eng. Des.61-62 (2002) 345-351.